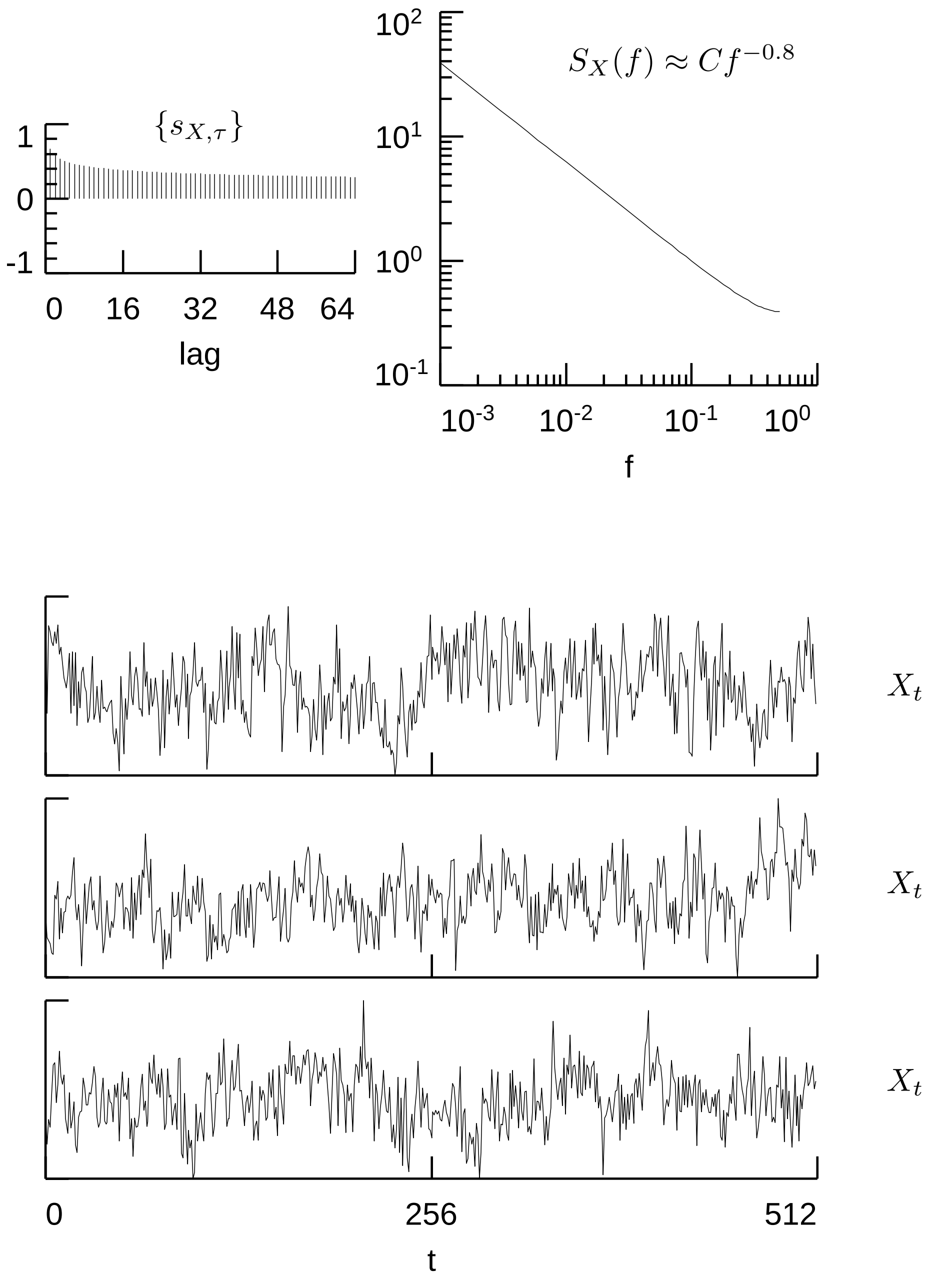

Figure 1. ACVS $\{s_{X,\tau}\}$, spectrum $S_X(\cdot)$ and three realization of an FD process with $\delta = 0.4$.

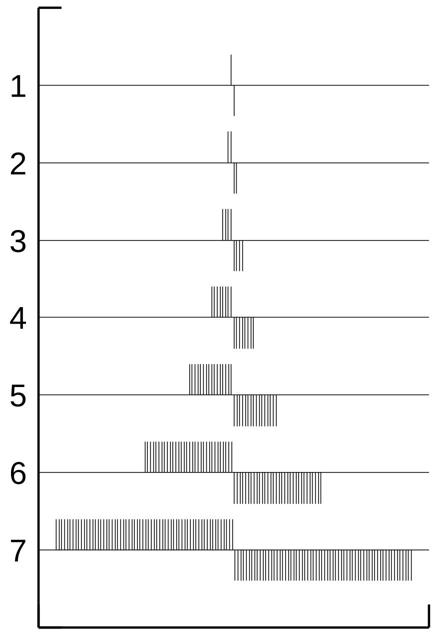

Figure 2. Haar wavelet filters for scales $\tau_j = 2^{j-1}$, $j = 1, 2, \ldots, 7$.

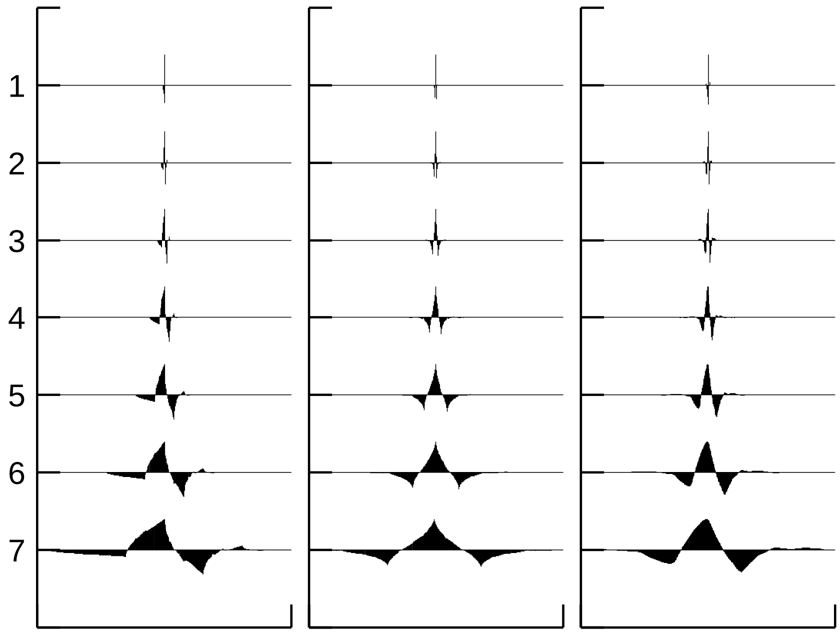

Figure 3. D(4), C(6) and LA(8) wavelet filters for scales $\tau_j = 2^{j-1}$, $j = 1, 2, \ldots, 7$.

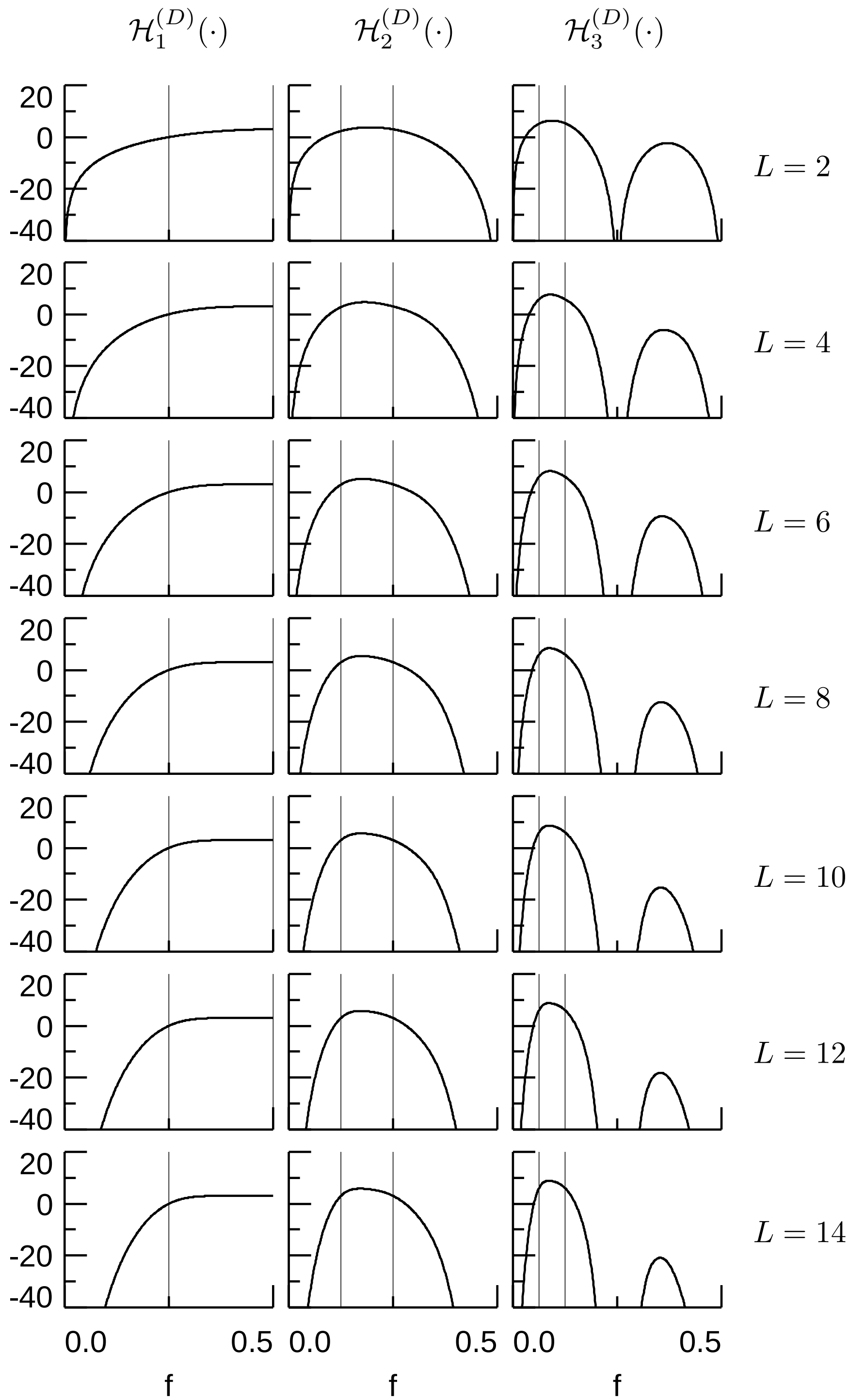

Figure 4. Squared gain functions $\mathcal{H}_j^{(D)}(\cdot)$, $j = 1, 2$ and 3 (left, middle and right columns, respectively), for Daubechies wavelet filters of widths $L = 2, 4, \ldots, 14$ (top to bottom rows, respectively). The two thin vertical lines in each plot delineate the nominal pass-band for the filter. The vertical axis is in decibels (i.e., we plot $10 \cdot \log_{10}(\mathcal{H}_j^{(D)}(f))$ versus f).

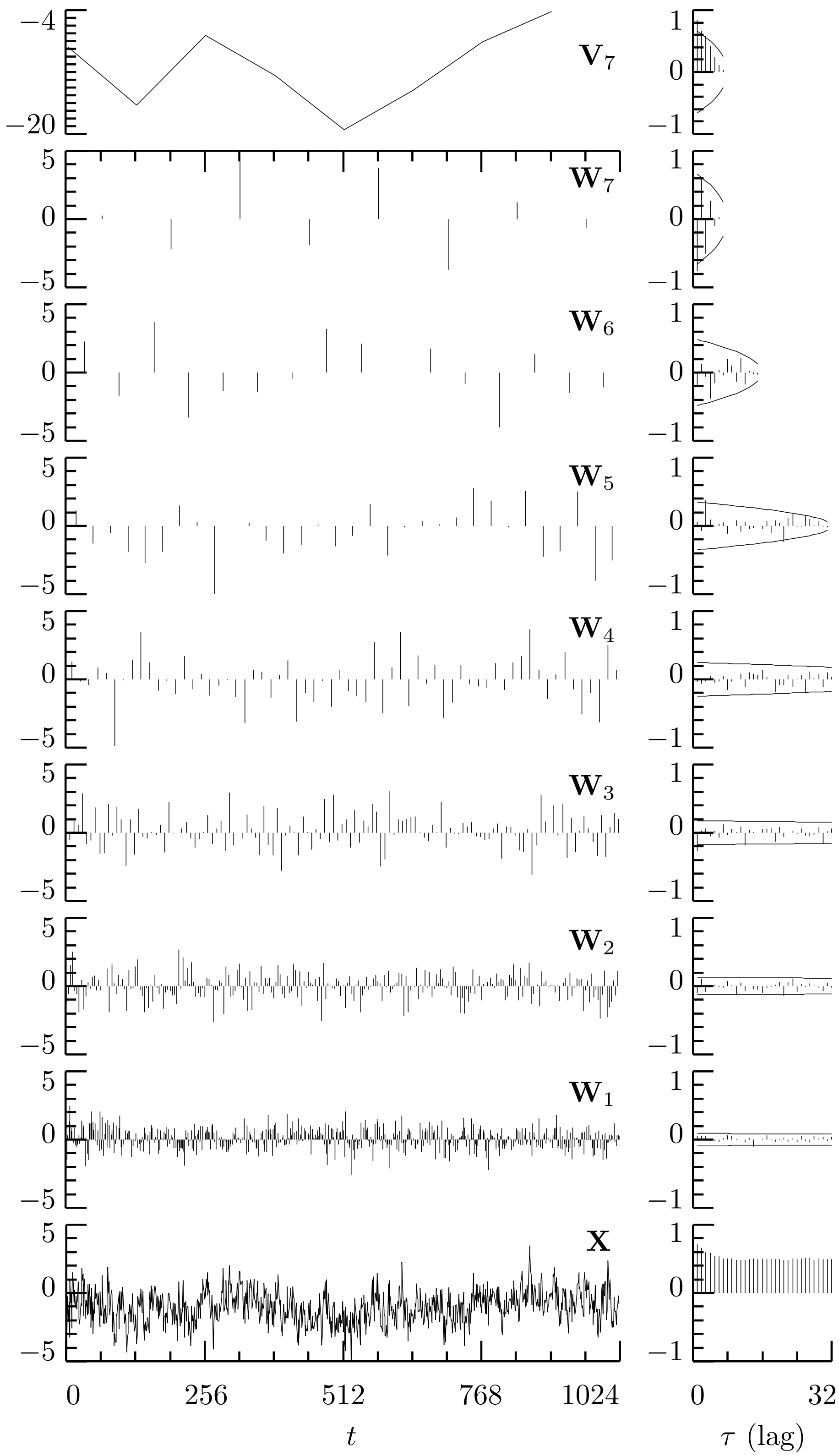

Figure 5. LA(8) DWT coefficients for simulated FD(0.4) time series and sample ACSs.

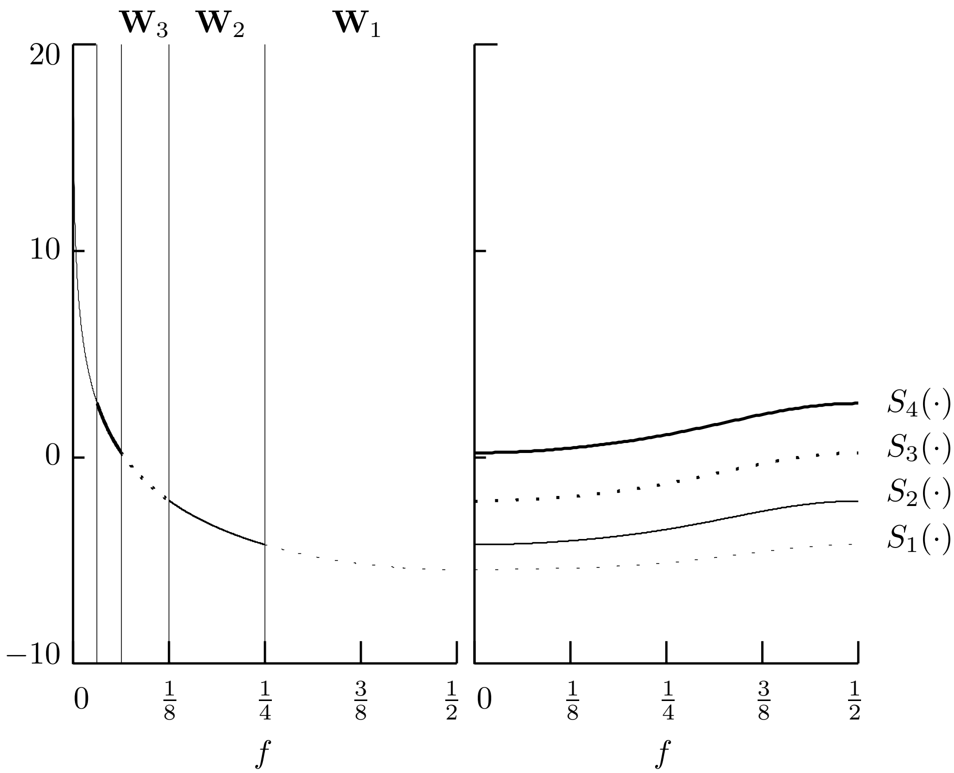

Figure 6. SDFs for an FD(0.4) process (left-hand plot) and for nonboundary LA(8) wavelet coefficients in $\mathbf{W}_1$, $\mathbf{W}_2$, $\mathbf{W}_3$ and $\mathbf{W}_4$ (right-hand). The vertical axis is in units of decibels (i.e., we plot $\log_{10}(S_X(f))$ versus f). The vertical lines in the left-hand plot denote the nominal pass-bands for the four $\mathbf{W}_j$.

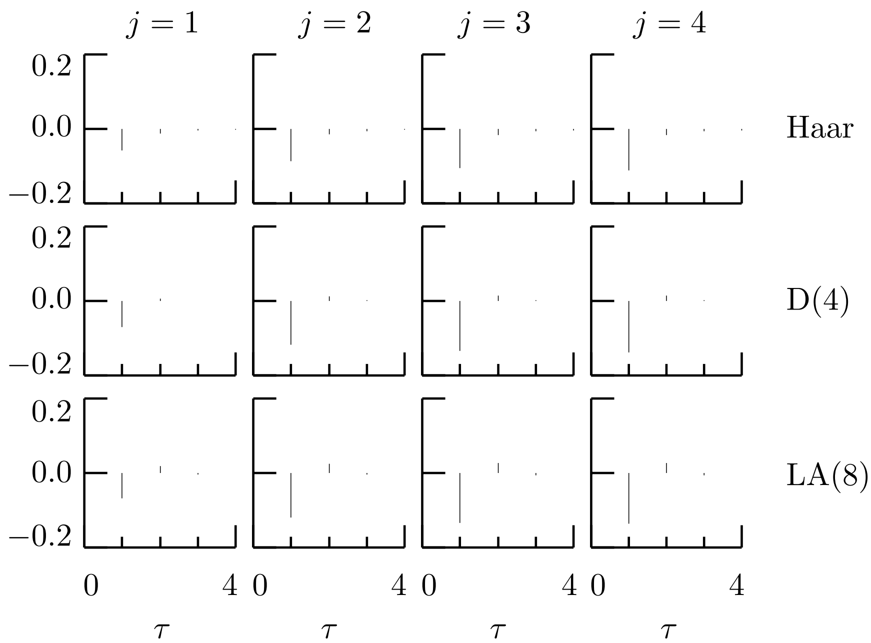

Figure 7. ACSs at $\tau = 1, \ldots 4$ for Haar, D(4) and LA(8) wavelet coefficients $W_{j,t}$, $j = 1, \ldots 4$, of an FD(0.4) process. The ACS values are plotted as deviations from zero (some are not visible because they are so close to zero).

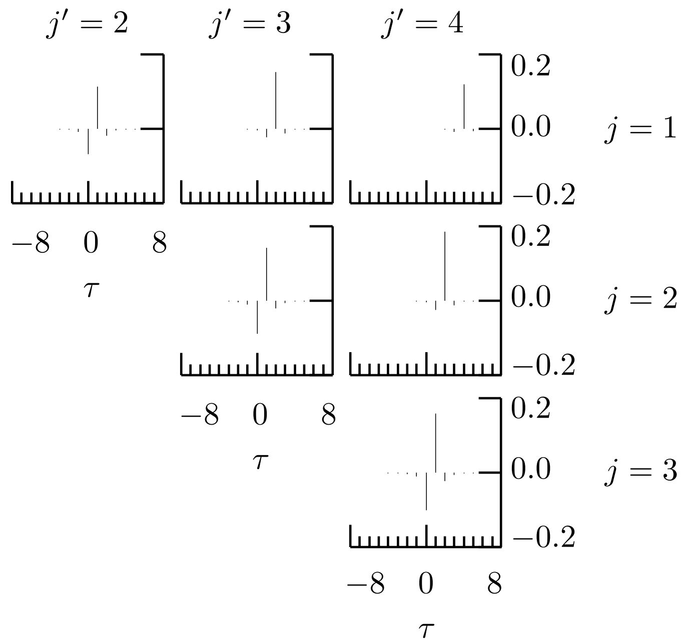

Figure 8a. Correlation between the Haar wavelet coefficients $W_{j,t}$ and $W_{j',t'}$ formed from an FD(0.4) process and for levels satisfying $1 \leq j < j' \leq 4$.

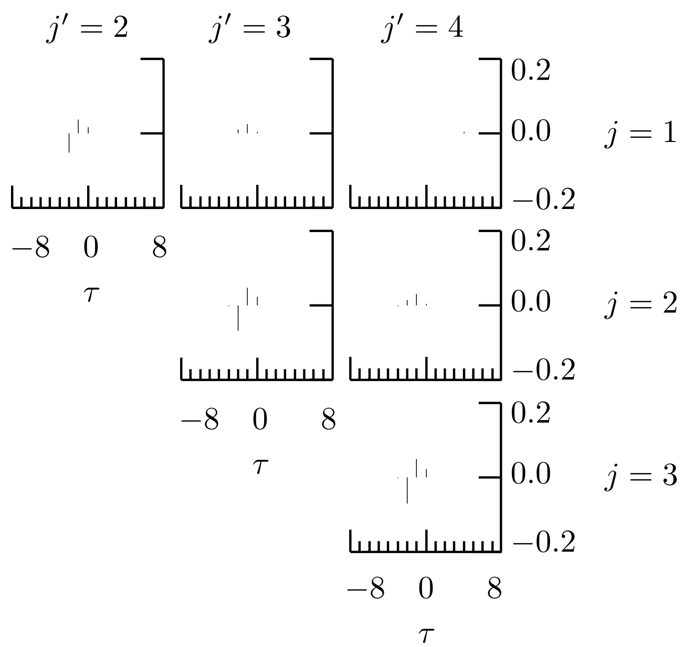

Figure 8b. As in Figure 8a, but now using the LA(8) DWT.

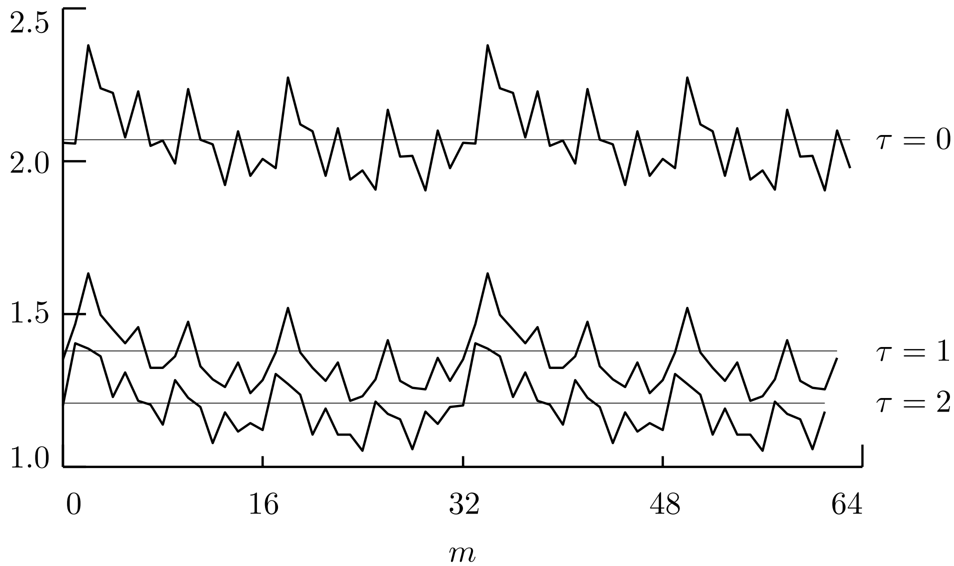

Figure 9. Diagonal elements $\Sigma_{\mathbf{Y},m,m+\tau}$ and $\Sigma_{\mathbf{X},m,m+\tau}$, $m = 0, \ldots, N-1-\tau$, of the covariance matrices $\Sigma_{\mathbf{Y}}$ and $\Sigma_{\mathbf{X}}$ (thick jagged curves and thin horizontal lines, respectively) for sample size $N = 64$ from an FD(0.4) process with $\sigma^2 = 1$ and with $\Sigma_{\mathbf{Y}}$ constructed using an LA(8) DWT. Three diagonals are plotted for each covariance matrix, namely, the main diagonal ($\tau = 0$) and the first two off-diagonals ($\tau = 1$ and 2). Whereas $\Sigma_{\mathbf{X}}$ exhibits the Toeplitz structure required for a stationary process, its approximation $\Sigma_{\mathbf{Y}}$ does not.

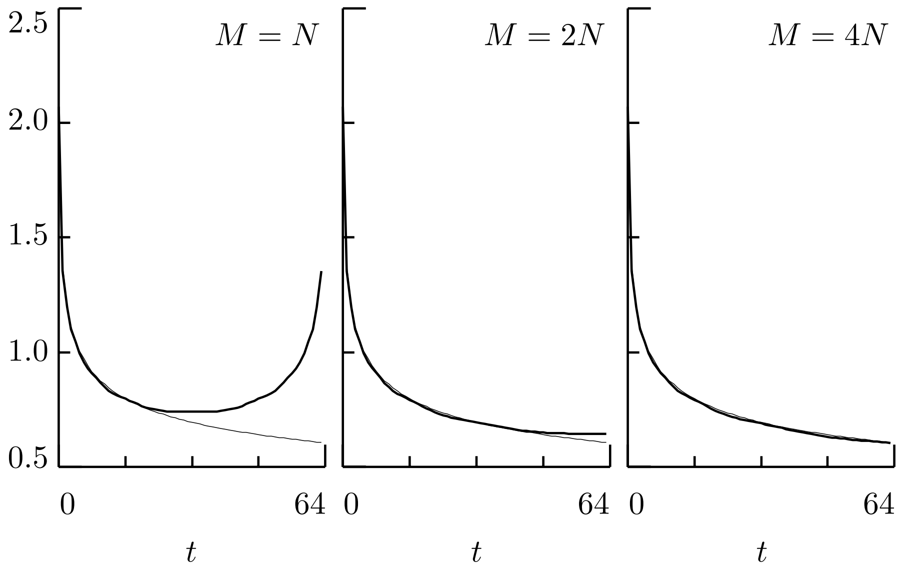

Figure 10. True ACVS (thin curves) and wavelet-based approximate ACVSs (thick) for an FD(0.4) process. The approximating ACVSs are based on an LA(8) DWT in which we generate a series of length M and then extract a series of length $N = 64$. As M goes from N to $4N$, the approximate ACVS gets closer to the true ACVS.

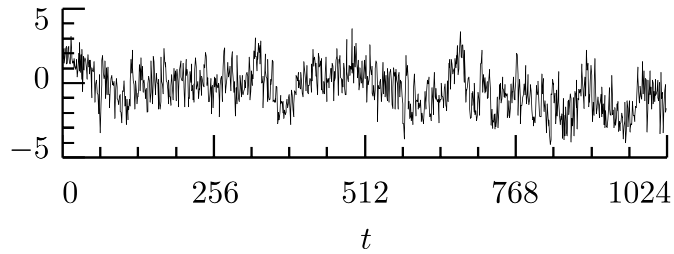

Figure 11. LA(8) wavelet-based simulation of a series of length $N = 1024$ from an FD process with zero mean and with parameters $\delta = 0.4$ and $\sigma^2 = 1.0$.

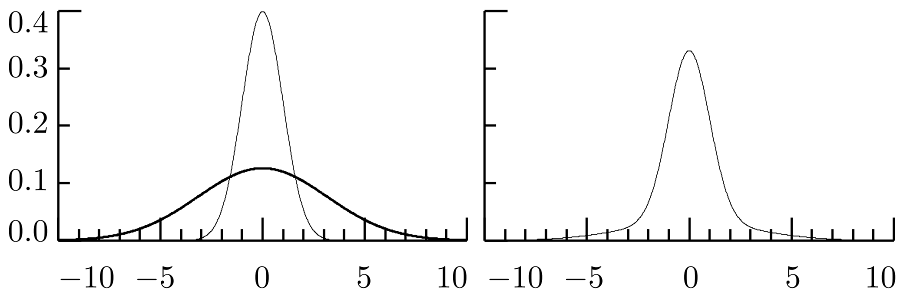

Figure 12. PDFs for $\mathcal{N}(0,1)$ and $\mathcal{N}(0,10)$ RVs (left-hand plot, thin and thick curves, respectively) and for an RV obeying a Gaussian mixture model (right-hand plot). The mixture PDF is non-Gaussian and is formed by adding the $\mathcal{N}(0,1)$ and $\mathcal{N}(0,10)$ PDFs, weighted by $p = 0.75$ and $1-p = 0.25$, respectively (adapted from Figure 1 of Chipman *et al.*, 1997).

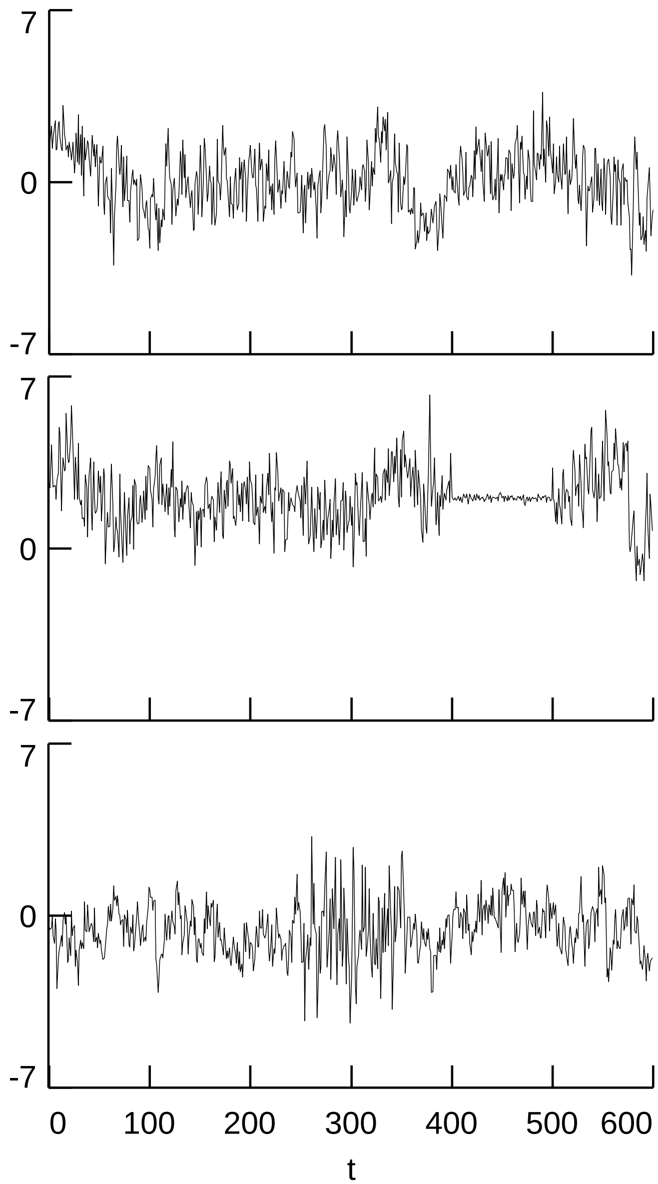

Figure 13. Three simulated time series generated using the wavelet-based scheme. The top series was constructed using homogeneous variances for each scale, while the bottom two series use inhomogeneous variances. The middle series has a quiesent period of about a hundred points, whereas the bottom has a noticeable burst of about the same duration. While all three series are realizations of stationary processes with spectra that are designed to approximate that of an FD process with $\delta = 0.4$, their marginal distributions obey quite different Gaussian mixture models (the distribution for the top series is in fact very close to Gaussian).

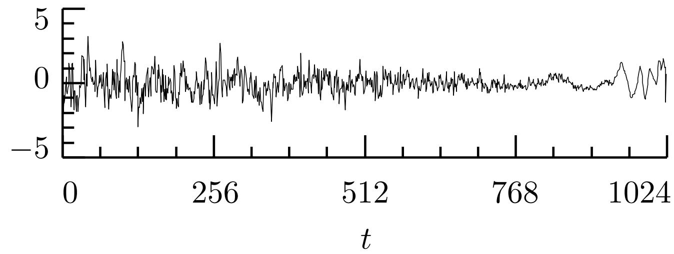

Figure 14. LA(8) wavelet-based simulation of a series of length $N = 1024$ from process with time varying statistical properties.

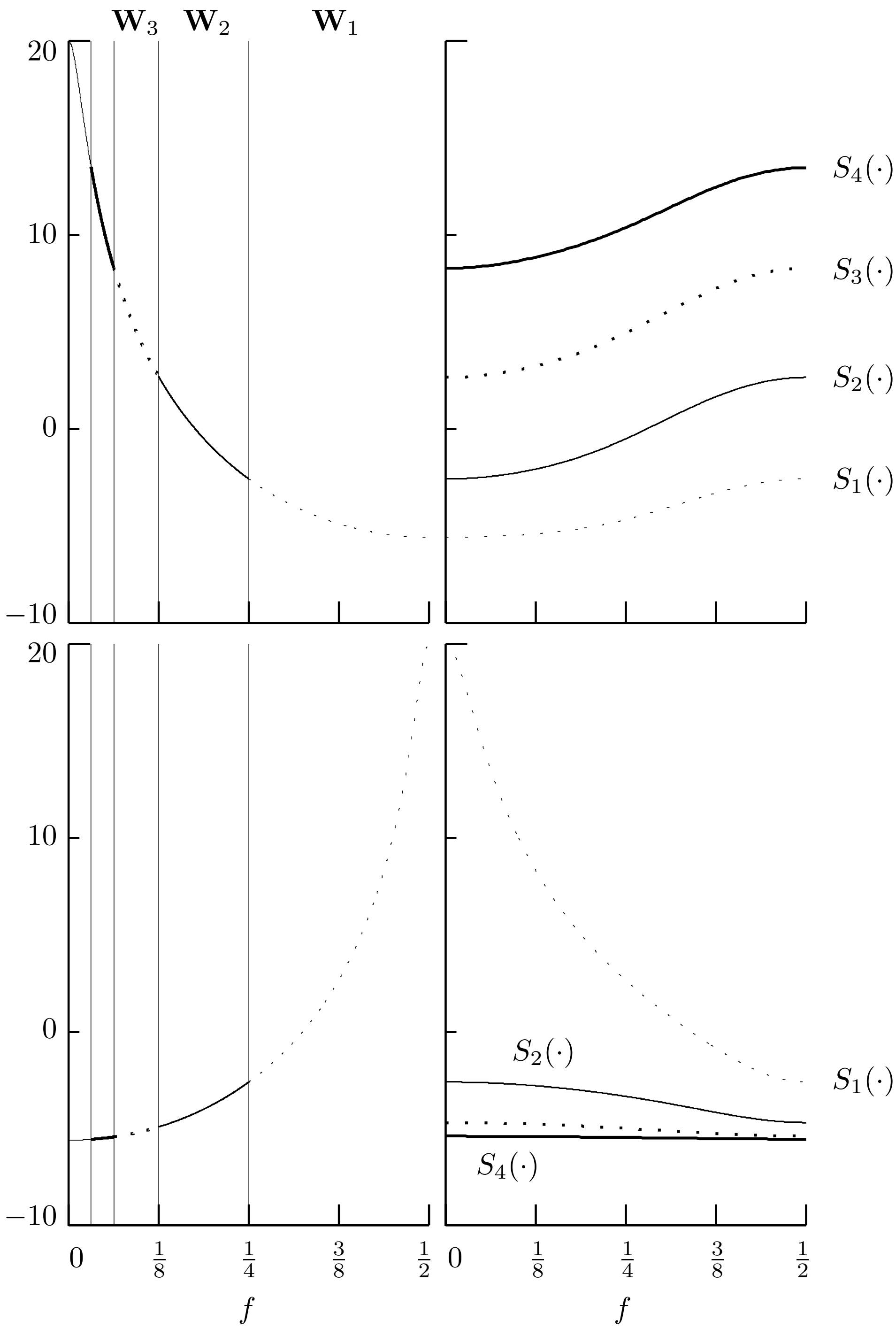

Figure 15. SDFs for AR(1) processes (top plot) with $\phi = 0.9$ (thick curve) and -0.9 (thin) and for corresponding nonboundary LA(8) wavelet coefficients in $\mathbf{W}_1$ to $\mathbf{W}_4$ (bottom four plots). The vertical axes are in decibels, and the vertical lines in the top plot denote the nominal pass-bands for the four $\mathbf{W}_j$.

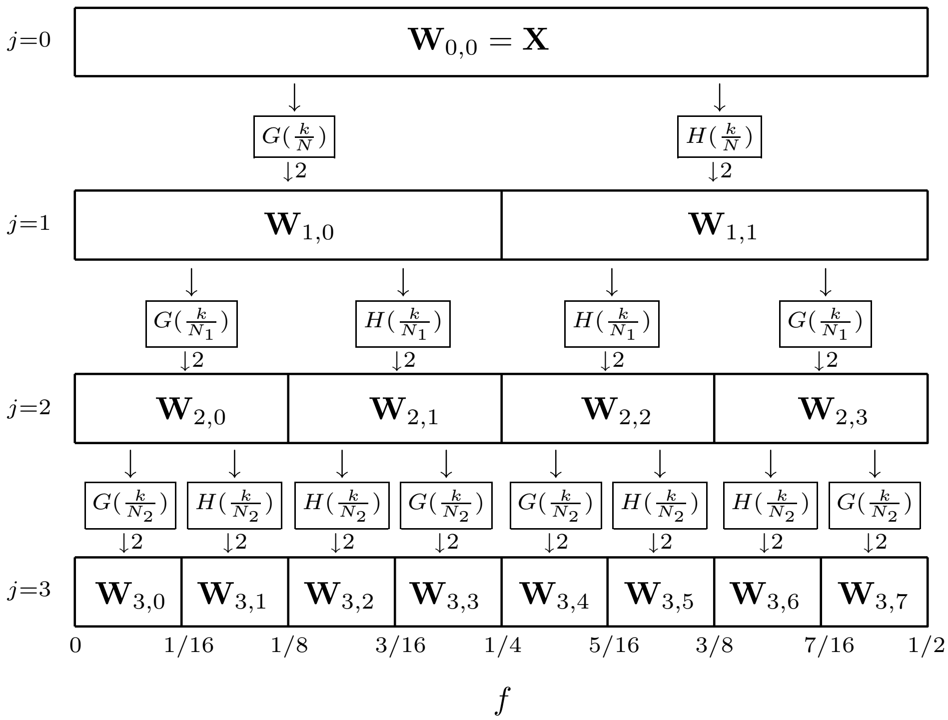

Figure 16. Flow diagram illustrating the analysis of $\mathbf{X}$ into $\mathbf{W}_{3,0}, \ldots, \mathbf{W}_{3,7}$ (recall that $N_j \equiv N/2^j$).

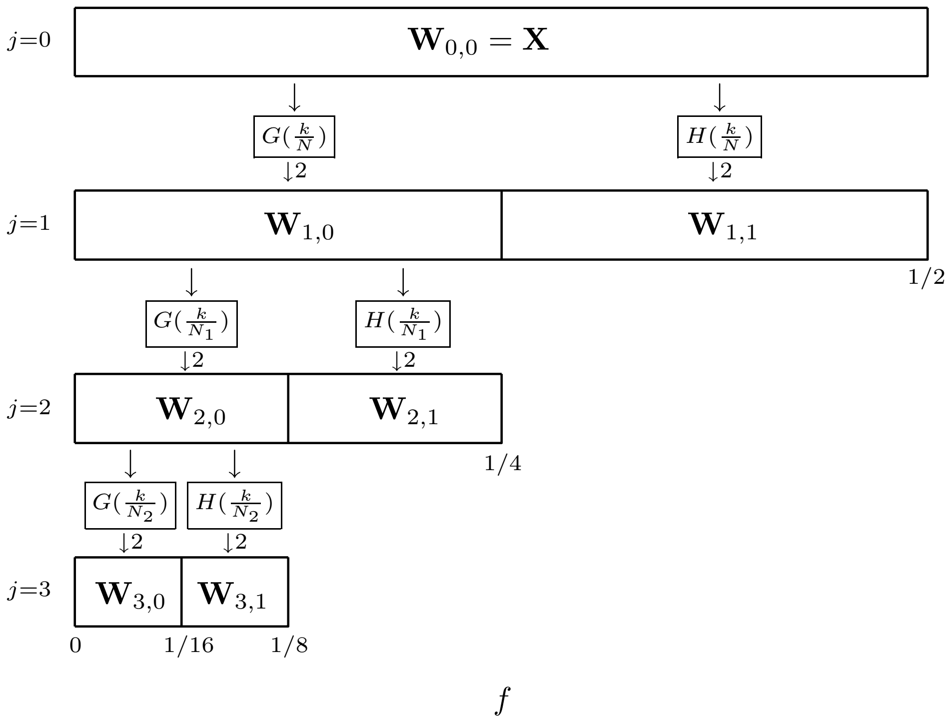

Figure 17. Flow diagram illustrating the analysis of $\mathbf{X}$ into $\mathbf{W}_{3,0}$, $\mathbf{W}_{3,1}$, $\mathbf{W}_{2,1}$ and $\mathbf{W}_{1,1}$, which is identical to a partial DWT of level $J_0 = 3$.

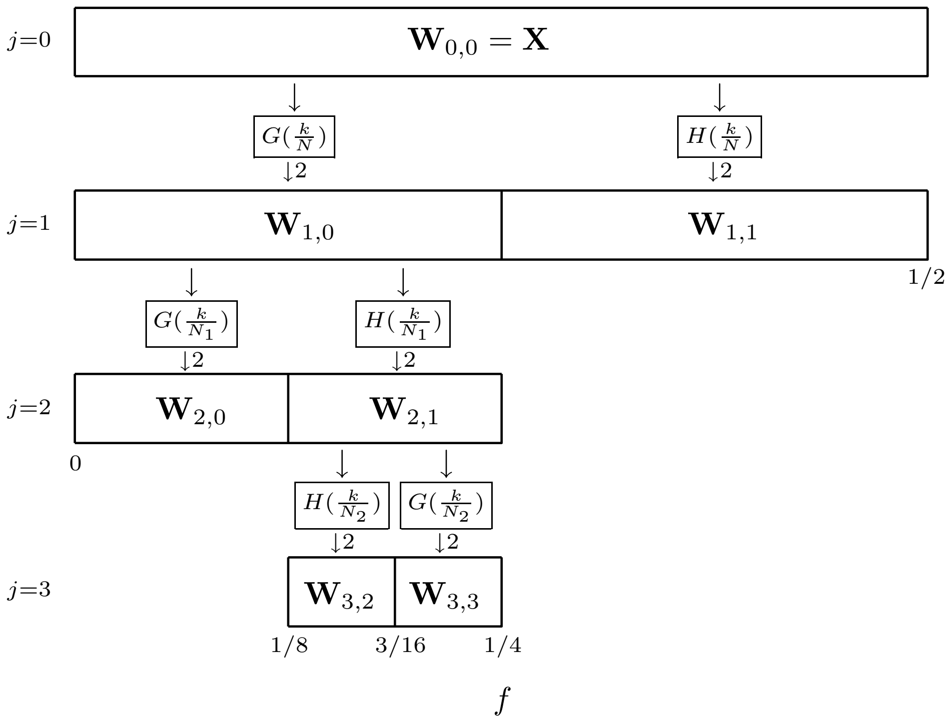

Figure 18. Flow diagram illustrating the analysis of $\mathbf{X}$ into $\mathbf{W}_{2,0}$, $\mathbf{W}_{3,2}$, $\mathbf{W}_{3,3}$ and $\mathbf{W}_{1,1}$, an arbitrary disjoint dyadic decomposition.